ORIGINAL

Observations of pockmark flow structure in Belfast Bay, Maine, Part 1: current-induced mixing

Christina L. Fandel[1,2] · Thomas C. Lippmann[1] · James D. Irish[1] · Laura L. Brothers[3]

Abstract Field observations of current profiles and temperature, salinity, and density structure were used to examine vertical mixing within two pockmarks in Belfast Bay, Maine. The first is located in 21 m water depth (sea level to rim), nearly circular in shape with a 45 m rim diameter and 12 m rim-to-bottom relief. The second is located in 25 m water depth, more elongated in shape with an approximately 80 m (36 m) major (minor) axis length at the rim, and 17 m relief. Hourly averaged current profiles were acquired from bottom-mounted acoustic Doppler current profilers deployed on the rim and center of each pockmark over successive 42 h periods in July 2011. Conductivity–temperature–depth casts at the rim and center of each pockmark show warmer, fresher water in the upper water column, evidence of both active and fossil thermocline structure 5–8 m above the rim, and well-mixed water below the rim to the bottom. Vertical velocities show up- and down-welling events that extend into the depths of each pockmark. An observed temperature change at both the rim and center occurs coincident with an overturning event below the rim, and suggests active mixing of the water column into the depths of each pockmark. Vertical profiles of horizontal velocities show depth variation at both the center and rim consistent with turbulent logarithmic current boundary layers, and suggest that form drag may possibly be influencing the local flow regime. While resource limitations prevented observation of the current structure and water properties at a control site, the acquired data suggest that active mixing and overturning within the sampled pockmarks occur under typical benign conditions, and that current flows are influenced by upstream bathymetric irregularities induced by distant pockmarks.

Introduction

Pockmarks are roughly conical depressions in the seafloor that are distributed in a variety of global geologic environments ranging from shallow coastal regions (e.g., Wildish et al. 2008; Brothers et al. 2011a, b), to deep offshore settings (e.g., Hovland and Judd 1988; Hovland and Svensen 2006). These crater-like features range in size from less than 1 m to over a kilometer in diameter. In Belfast Bay, located in the northwestern quadrant of Penobscot Bay in central Maine, USA, there exists an extensive field of over 1,700 pockmarks within a 25 km² area (Fig. 1; Scanlon and Knebel 1989; Andrews et al. 2010). Methane release from Holocene estuarine mud is considered to be the primary mechanism of pockmark formation in Belfast Bay, yet the relative degassing history and maintenance mechanisms of the pockmarks remain unresolved (Kelley et al. 1994), similar to other areas worldwide (e.g., Scanlon and Knebel 1989; Christodoulou et al. 2003). Although timing and activity of pockmark formation is highly uncertain, many pockmarks are believed to have been inactive for long periods of time (perhaps years or more; e.g., Kelley et al. 1994). Thus, the question remains as to why inactive pockmarks do not—over time—fill in with sediments, and for non-actively venting pockmark fields, it is not clear what the mechanisms are for long-term maintenance.

✉ Thomas C. Lippmann
lippmann@ccom.unh.edu

[1] University of New Hampshire, Center for Coastal and Ocean Mapping, 24 Colovos Rd., Durham, NH 03824, USA

[2] Present address: Hydrographic Surveys Division, Office of Coast Survey, National Oceanic and Atmospheric Administration, 1315 East-West Hwy, Silver Spring, MD 20910, USA

[3] U.S. Geological Survey, 384 Woods Hole Rd., Woods Hole, MA 02543, USA

Springer

Fig. 1 Overview map of Belfast Bay, Maine, with the approximate location of each sampled pockmark (*green box*). Weather stations 1 and 2 (*blue triangles*) are located approximately 2.4 km east of Belfast and Searsport, Maine, respectively
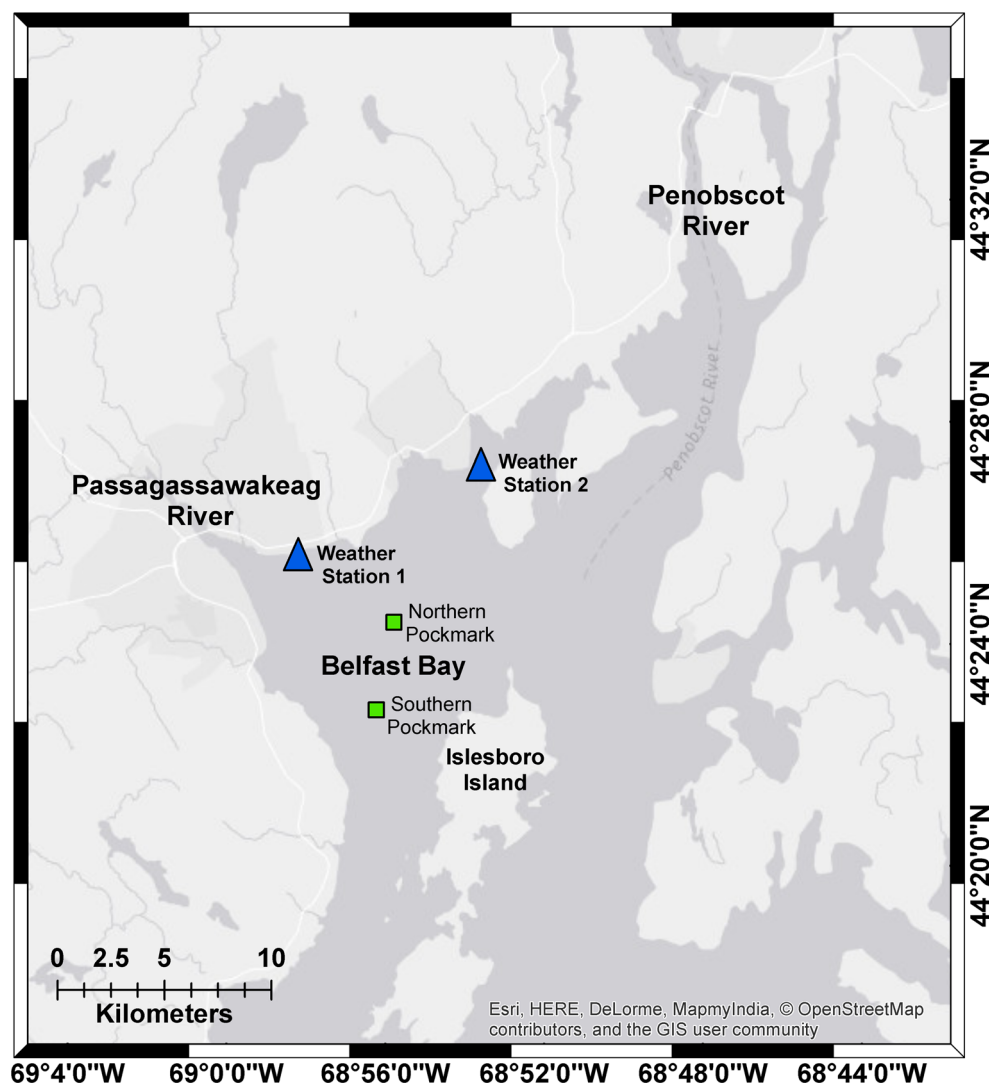
Although much research has addressed pockmark formation, specifically in Belfast Bay (e.g., Scanlon and Knebel 1989; Kelley et al. 1994; Rogers et al. 2006; Brothers et al. 2012), few studies have focused on direct observations of circulation, mixing, and sediment characteristics within pockmarks. One notable exception is a recent field study by Pau and Hammer (2013) who include observations of sediment grain size and geochemical composition, as well as acoustic backscatter and flow above pockmarks in Oslofjord, Norway. Their work suggests that deposition in pockmarks may be determined by the relative importance of bedload and suspended sediment transport patterns, or by biological activity (i.e., swimming fish) that induce diurnal circulation patterns over the sampled pockmark (Pau and Hammer 2013). Although lack of horizontal and vertical flow measurements within the depths of the pockmarks prevent direct observation of the deep circulation or mixing of fluid into and out of the depressions, their work suggests that pockmarks in Oslofjord may be maintained by modern conditions. Seismic records in

the North Sea show stratigraphic sediment layering consistent with elongation of initially circular pockmarks, and subsequent coalescing of neighboring pockmarks that form km long (multiple) furrows suggesting that post-formation processes modify pockmark fields through sediment transport mechanisms (Kilhams et al. 2011). However, more field studies that observe flows and mixing within the pockmarks are needed to improve understanding of sediment transport mechanisms for post-formation pockmarks, better constrain models for age approximation, and guide models for improved estimation of mixing and nutrient distribution within individual pockmarks (e.g., Gay et al. 2005; Hovland et al. 2005; Wildish et al. 2008; Ritt et al. 2011).

In Part 1 of this study (this paper), field observations obtained within the depths (near the bottom) and the rim of two pockmarks in Belfast Bay, Maine, are presented and discussed. Both pockmarks show evidence of active mixing of water above and below the rim, and a vertical flow structure with boundary layers induced by both internal pockmark

circulation and external flows influenced by upstream bathymetric irregularities. In Part 2 (Fandel et al. 2016a), circulation patterns and horizontal shear layer growth within the pockmarks are shown to be consistent with open cavity flows and previously modeled flow patterns (Brothers et al. 2011a; Pau et al. 2014). Finally, in Part 3 (Fandel et al. 2016b), observed horizontal and vertical currents are examined in conjunction with the cohesive sediment characteristics to characterize periods of sediment resuspension and deposition within and around the pockmarks.

Materials and methods

Field observations of the temperature, salinity, density, and current structure were obtained over the rim and center of two pockmarks with conductivity, temperature, and depth (CTD) casts and bottom-mounted, upward-looking acoustic Doppler current profilers (ADCPs). Candidate pockmarks were selected from a 5 by 5 m resolution bathymetric map of Belfast Bay produced from interferometric sonar data acquired by the U.S. Geological Survey in cooperation with the University of Maine in 2006 and 2008 (Brothers et al. 2011a). Characterized as a shallow estuarine environment (10–50 m water depths), Belfast Bay receives fresh-water input from the lower flow Passagassawakeag River to the northwest and the higher flow Penobscot River to the northeast (US Geological Survey 2010). Pockmark morphology transitions from a nearly circular shape in the shallower, northern region to a more elongated shape in the deeper, southern region, where the bay significantly constricts. Two pockmarks were selected based on proximity to other pockmarks, depth restrictions of the instrumentation, and characteristic morphology (Fig. 2). A geographic right-handed coordinate system is adopted with vertical datum at mean sea level and z-coordinate positive upward. Water depths are reported as positive values.

The first pockmark selected was nearly spherical with a 45 m diameter at the rim, and located in 21 m water depth with 12 m relief (depression) from the rim to the bottom. The second selected pockmark is located to the south in 25 m water depth, and is more elongated with 80 m major axis and 36 m minor axis lengths, and 17 m relief below the rim. The northern pockmark is located near a complex convergence zone of tidal currents flowing around Islesboro Island, whereas the southern pockmark is located in a narrower channel to the west of Islesboro Island where tidal currents are stronger and more aligned with the direction of the channel. Data were obtained in 2011 during rising spring tides at the northern pockmark from 26 July 1500 Eastern Standard Time (EST) through 28 July 1100 EST (Julian days 207.8–209.6), and in the southern pockmark from 28 July 1700 EST through 30 July 1000 EST (Julian days
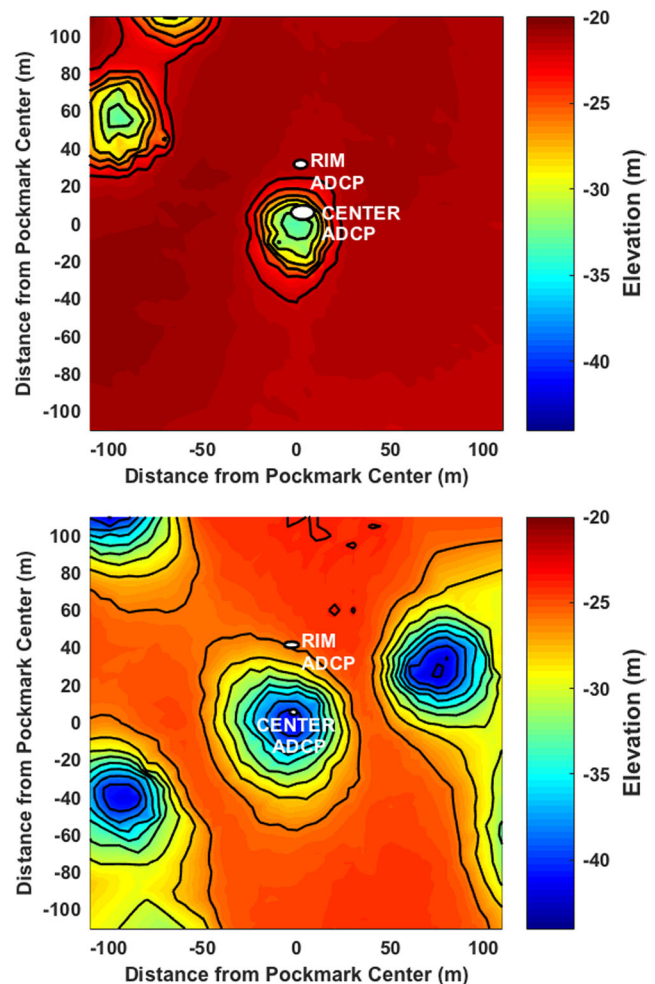

Fig. 2 Color-filled contour plots show bathymetric data collected over the northern (*top panel*) and southern (*bottom panel*) pockmark with x and y axes showing the estimated distance from the center of each pockmark. *White dots* Approximate location of each current meter mount along the rim and center of each pockmark, with associated uncertainty denoted by the size of each dot. Elevations are referenced to mean sea level

209.9–211.6). Field observations were not acquired at a control site due to resource limitations.

Hourly averaged wind speed, direction, and gust speed from meteorological stations located onshore near the townships of Belfast and Searsport, Maine (Fig. 1) were collected and distributed by Weather Underground, Inc. (2011). Anemometers were located about 30 m and 15 m above mean sea level at the Belfast and Searsport weather stations, respectively. The general agreement between the two distant sites suggests that the length scales of the variability would not greatly influence the interpretation of the results. Significant wave heights were generally small (about 0.25 m) in Penobscot Bay, and characterized by high-frequency sea waves (with short periods of order 1–3 s) rapidly spun up and down by the local diurnal wind patterns, and with limited swell (with longer periods of order 5–10 s) from distant sources.

Bathymetry

A dense bathymetric survey was conducted aboard the R/V Cocheco for a complete tidal cycle by making many (of order 50) criss-crossing transects over each pockmark (Fig. 2). Bathymetric data were acquired using a side-mounted 200 kHz ODOM THP 200 single-beam echo sounder pinging at about 10 Hz. Sub-meter positioning accuracy was achieved using an Omnistar 8200 HP differential global positioning system (GPS) that continually received differential GPS corrections via satellite transmission. Bathymetric data were post-processed and gridded to 2.5 m resolution using Computer Aided Resource Information System (CARIS) Hydrographic Information Processing System (HIPS) 7.0 software, and referenced to mean sea level using time- and range-corrected water level observations from the National Oceanic and Atmospheric Administration (NOAA) tide station 8418150 located to the south in Portland, Maine.

Current observations

Three-component current velocity profiles were concurrently acquired at the rim and center of each pockmark over the 48 h sampling period. Upward-looking RD Instruments (RDI) Workhorse 300 kHz ADCPs were installed on triangular aluminum frames about 1 m on a side with height of 0.52 m and 0.63 m above bottom in the rim and center of the pockmarks, respectively. Velocity profiles were sampled in regularly spaced 0.5 m bins through the water column beginning 2.37 m (rim location) and 2.24 m (center location) above the seafloor. The ADCPs sampled currents in each bin at 1.6 s intervals and then averaged over 5 minute periods. The center current meter mount additionally housed a Nortek Aquadopp acoustic current meter sampling at 0.7 m above the seafloor at 1 Hz, and recording near-bed mean currents over 1 minute periods. Currents were further averaged after data collection over 1 h intervals and over four adjacent vertical bins to yield mean three-component current profiles with 0.0025 m/s accuracy (RD Instruments 2005). All ADCP and Aquadopp data were synchronized to within 1 s.

ADCP mount locations (Fig. 2) at the rim of each pockmark were identified from acoustic backscatter data obtained with the ODOM sonar. However, the center ADCP mounts were not delineated in the backscatter owing to the steep sidewalls of the pockmarks. These positions were estimated from surface GPS positioning at the time of deployment, and from differences (offsets) between the backscatter-derived and GPS-derived estimates at the rim (Fig. 2). The GPS-derived positions were estimated by relating the time-averaged GPS position and orientation of the moored vessel at the time of deployment to the spatial distance between the vessel's GPS antenna location and A-frame. The relative offsets between the backscatter-estimated and GPS-estimated position of the

rim ADCPs were applied to the GPS-estimated position of the center ADCP. The associated uncertainty of each center location was determined by the quadratic sum of uncertainty sources, and estimated to be within about ±3.5 m and ±1.8 m horizontally at the northern and southern pockmark, respectively. The location of the center mounts in each pockmark is along the sloping northeastern sidewall, and is consistent with internally measured orientation angles recorded by the ADCPs.

The estimated ADCP locations and approximate beam angles, based on observed tilt angles measured with accuracy of ±0.5°, are shown in Fig. 3 along a north–south cross-sectional transect of the bathymetry at each pockmark. These bathymetric profiles are relative to mean sea level and indicate an approximate north–south symmetry of each pockmark. Note that the morphology at the rim of the southern pockmark is more elongated (length-to-width ratio ~2.2) than the northern pockmark (length-to-width ratio ~1.2). The rim mounts were deployed on nearly level ground, with a tilt angle of 2° and 7° for the northern and southern pockmark, respectively. This near-level deployment configuration resulted in all four acoustic beams of the RDI ADCP extending to the sea surface, and thus the current structure was resolved to within a short distance (1–2 m) of the surface. The center mounts were oriented at a significant angle of about 24° and 17° within the northern and southern pockmarks, respectively. These tilt angles were internally accounted for within each current meter sensor when resolving the orthogonal velocity components. However, as a consequence of the oblique orientation of the center ADCP, the four acoustic beams extended to different elevations within the water column and did not reach the sea surface. Bin locations above the maximum elevation sampled by all four beams were eliminated, allowing currents to be resolved within 4 and 8 m below the surface over the northern and southern pockmark, respectively.

CTD observations

Hydrographic casts were conducted using a Seabird 19 CTD profiler at locations near the center of each pockmark on approximately 2 h intervals spanning a single daytime tidal cycle to assess the time-varying temperature, salinity, and density structure of the water mass over each pockmark. The conductivity and temperature sensors of the CTD were assumed to be accurate within 0.001 S/m and 0.01 °C, based on manufacturers specification. In addition, seawater temperature was averaged over 5 minute periods at the ADCP transducer locations in the Nortek and RDI instruments with accuracies of 0.1 °C and 0.4 °C, respectively, and compared in situ with the CTD observations. It should be noted that the temperature gauge in the center pockmark ADCP is located externally and responds very quickly to changes in water temperature,
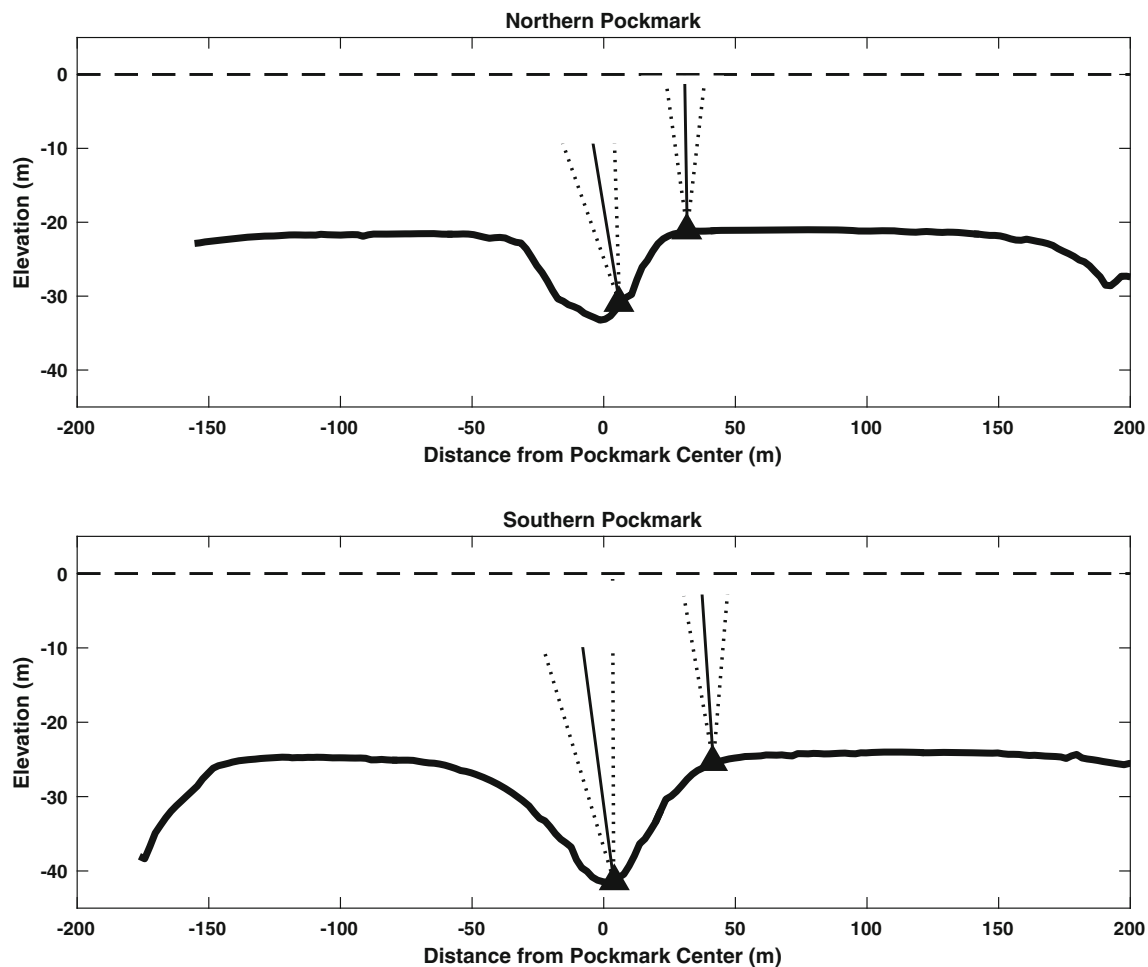
Northern Pockmark

Southern Pockmark

Fig. 3 N–S cross-sectional view of bathymetry across each pockmark, with the x axis indicating the distance from the approximate pockmark center and the y axis indicating elevation (in m) relative to mean sea level. *Gray triangle* Approximate location of each current meter mount. *Solid*

and dashed lines Path of the acoustic beams from the current meter mounts (with width between dashed lines to scale). Current data collected at ranges greater than the maximum distance reached by all acoustic beams were eliminated

whereas the temperature gauge in the rim ADCP is located internally and responds more slowly.

Results

Environmental conditions and depth-averaged currents

Time series of depth-averaged currents and wind conditions observed during the field experiment are shown in Fig. 4. Hourly averaged wind speed, direction, and gusts are indicated for wind stations in Belfast and Searsport. Observed winds showed variations on diurnal timescales with speeds increasing daily in the late afternoon (likely due to differential solar heating and cooling over land and ocean). Wind directions point toward the direction from which the winds were coming, and in large part were determined by weak frontal systems that caused abrupt 180° changes every couple of days. Winds rotated from northeast to southwest during the northern

pockmark sampling period, and oscillated between northeast and southwest during the southern pockmark sampling period.

Current magnitude and direction (points in the direction of the flow) are depth-averaged over three layers: a surface layer extending from near the sea surface to the approximate average depth of the thermocline (about 8 m), a mid-water layer extending from the thermocline to the rim, and a deep layer extending from the rim to the bottom of the pockmark (Fig. 4). Upper-water column currents range in magnitude from 0 to 0.25 m/s, but are typically in the range 0.05 to 0.10 m/s, and are primarily tidal with near-surface flow modified by wind-driven currents. Mid-water column currents are tidally dominated, particularly in the southern pockmark. Mid-water column currents over the northern pockmark are more variable, being influenced by wind-driven stress at the surface as well as by converging tidal currents around Islesboro Island. Current magnitudes in this layer range from 0 to 0.20 m/s, and are sometimes stronger than the surface flows creating a sub-surface current maximum. Observations of similar depth-
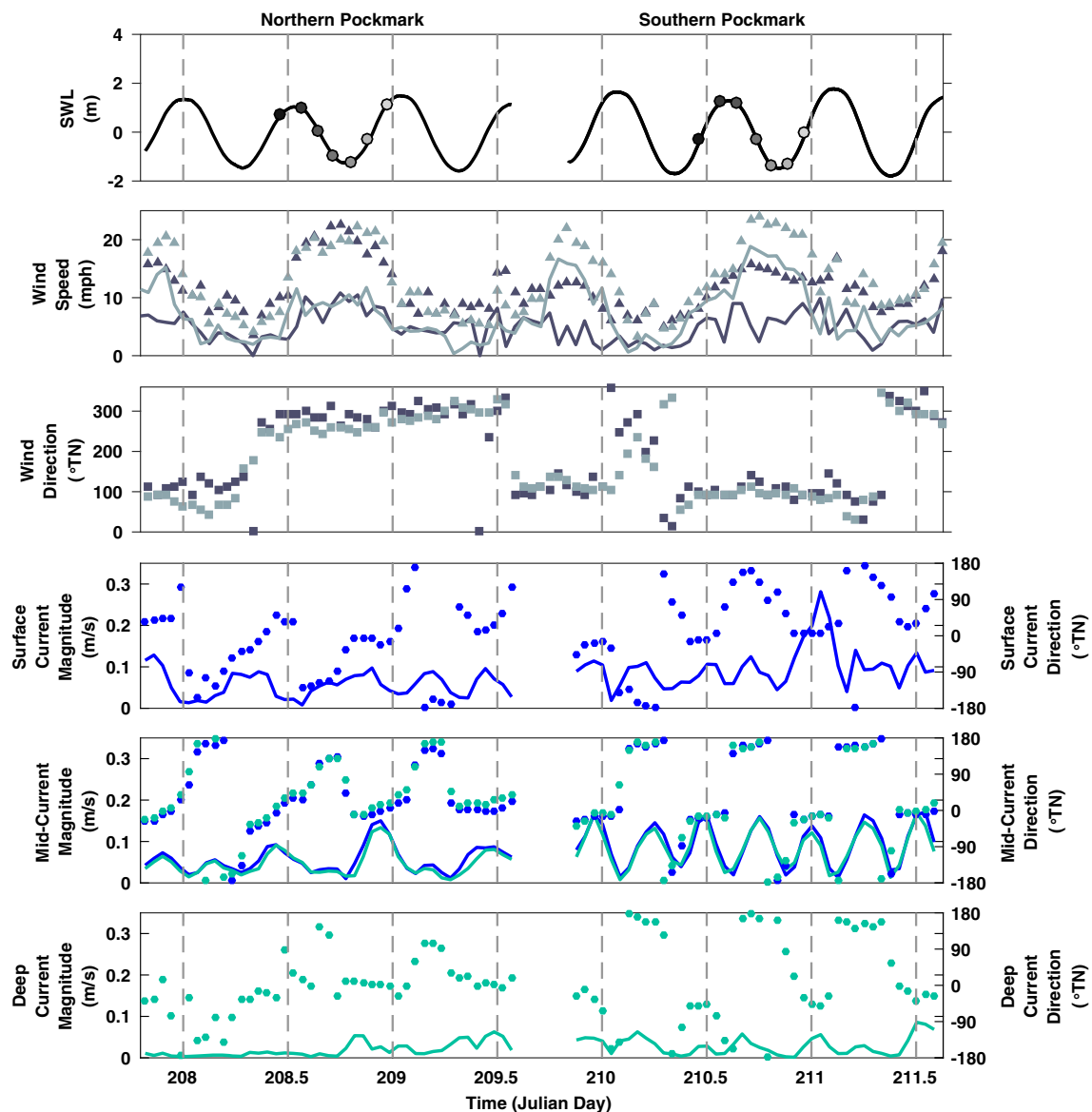
Fig. 4 Time series of sea surface elevation (top panel), winds (next two panels), and depth-averaged currents (bottom three panels) during the northern and southern pockmark sampling periods. Time on the x axis is 2011 Julian Days. Mean sea surface elevation is from bottom pressure data and shows the times (*circles*) of the CTD casts. Wind speed and direction (degrees true north) were obtained from meteorological stations near Belfast (*light gray*) and Searsport (*dark gray*). Triangles indicate hourly wind gusts. Hourly averaged current magnitude (*lines*) and direction (*dots*) are depth-averaged over the surface, mid, and deep layers, delineated by the average thermocline (8 m) and rim depths (21 and 24 m). Data displayed in *blue* (*teal*) were obtained from the current meter mount located in the rim (center) of either pockmark

averaged currents over the rim and center of each pockmark suggest a nearly uniform depth-averaged horizontal flow field over the pockmarks. The depth-averaged currents in the deep layer are much weaker, ranging from 0 to 0.05 m/s, decay with depth, and do not always show strong tidal oscillations.

Salinity and temperature observations

Salinity and temperature, and density profiles obtained from the CTD casts are shown in Figs. 5 and 6, respectively. The presence of a strong thermocline, halocline, and pycnocline indicate a highly stratified upper water column that evolves

through the tidal cycle and diurnal solar heating. Salinity increases with depth in the upper water layer (indicating the presence of fresh water river outflow), and is constant below the bottom of the halocline (about 10–13 m depth). Sharp variations in salinity occur between 5 m and 12 m depths below the surface, and may represent active mixing by surface processes or an advected flow from a previous mixing event. Temperature profiles show diurnal heating, with a characteristic deepening of the thermocline around mid-day. Uniform temperature and density profiles are observed to extend from a few meters above the rim to the bottom, suggesting a homogeneous, well-mixed deep layer throughout the pockmark.
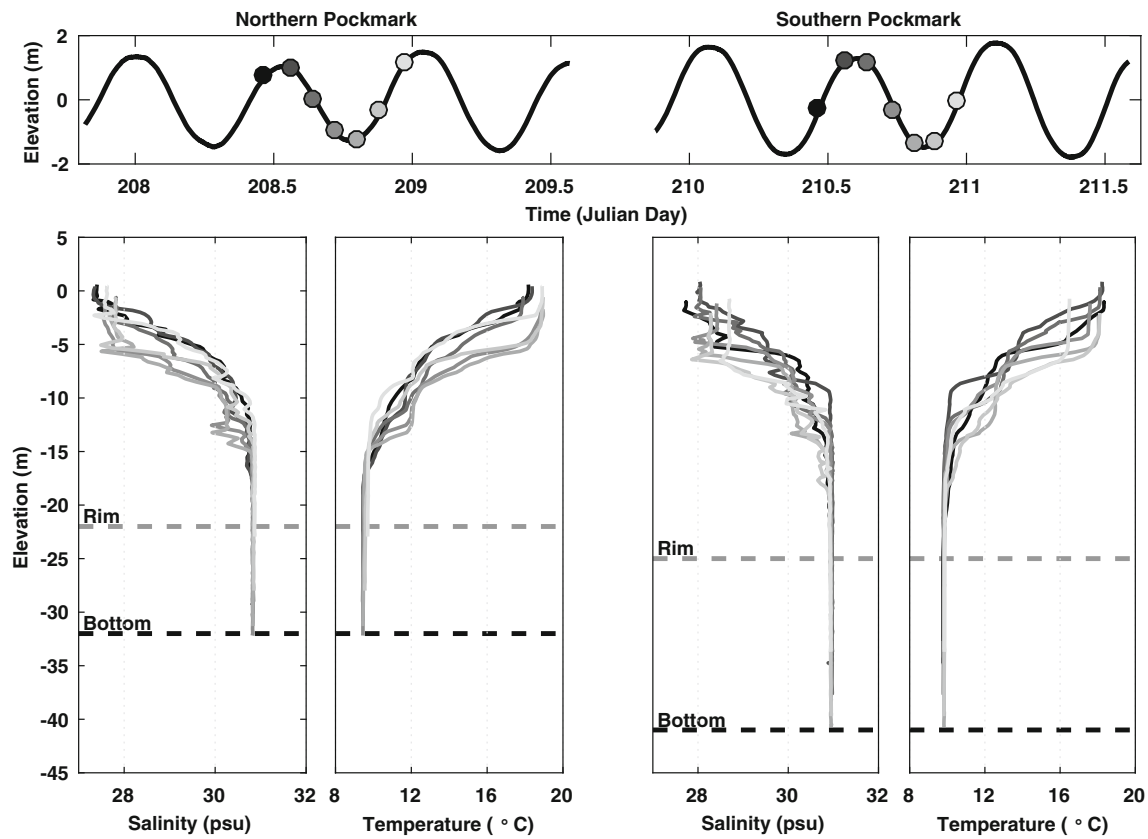
Fig. 5 Salinity and temperature profiles acquired over the center of the northern (*left panels*) and southern (*right panels*) pockmark. *Top panel* Tidal observations during the moored current meter sampling period: *gray dots along tidal wave* time at which the individual CTD casts were acquired (with the shade of gray corresponding between the dots and lines). *Horizontal dashed gray and black lines* Depth of the rim and bottom of each pockmark

Fig. 6 Density profiles acquired over the center of the northern (*left panel*) and southern (*right panel*) pockmark. *Top panel* Tidal observations during the moored current meter sampling period: *gray dots along tidal wave* time at which the individual CTD casts were acquired (with the shade of gray corresponding between the dots and lines). *Insets* Temporal evolution of each density profile. *Horizontal dashed gray and black lines* Depth of the rim and bottom of each pockmark
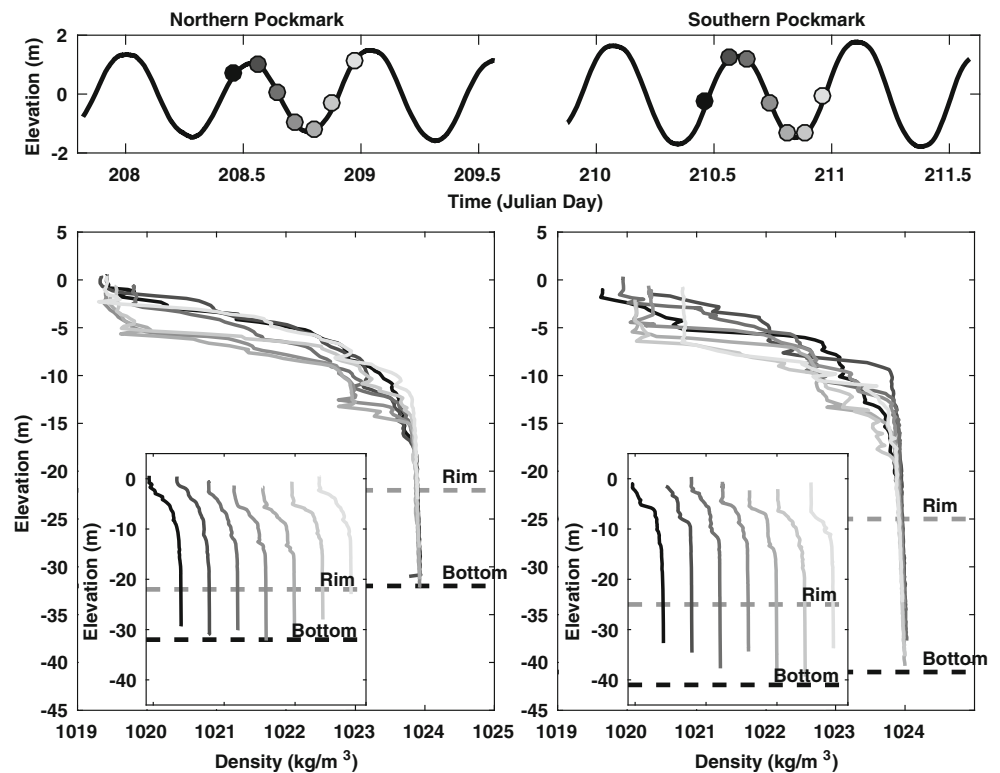
Time series of near-seabed temperature recorded by the rim and center ADCPs are shown in Fig. 7. A 0.3 °C rise in temperature was recorded at the rim and center of the northern pockmark beginning on Julian day 208.8, and occurs over an approximately 6 h time period. This nearly simultaneous rise in temperature at both ADCP locations was also observed by the last two CTD casts, and indicates that the water temperature rapidly increased uniformly across the pockmark and extended from the rim to the bottom of the pockmark. The time lag in temperature between the rim and center ADCPs is likely the result of the different response times of the instruments, whereby the externally located temperature sensor at the center ADCP mount responds more quickly to changes in temperature than the internally located temperature sensor at the rim. Based on observed flow speeds and direction during this period, the time lag in temperature is not likely a result of a frontal system traveling through the pockmark.

Also shown in Fig. 7 are depth-averaged vertical velocities in the deep layer. Up- and down-welling events with magnitudes of about 0.01–0.015 m/s are coincident with the rise in temperature, and suggest that a strong vertical mixing event (or flow of water down into the pockmark) extended from the center of the pockmark to above the rim (Fig. 7). The initial rise in temperature occurred coincident to relatively strong upward-directed (positive) vertical velocities depth-averaged below the rim, and is followed by a similarly strong down-welling period. At the southern pockmark, a gradual rise in temperature was measured at both the rim and center ADCP locations, and was associated with a weak, net downward

velocity over the duration of the deployment period consistent with a slow, persistent circulation of external water above the rim into the depths of the pockmark.

Mean current vertical structure

The temporal evolution of the vertical structure of hourly averaged vertical velocities measured from the center ADCP in both the northern and southern pockmarks is shown in Fig. 8. Typical vertical velocities are in the range of ±0.02 m/s, and show strong vertical structure and temporal variability. The data indicate episodic up- and down-welling events over the center of each pockmark that extend from above the rim well into the pockmark.

Two up-welling events were observed during the northern pockmark sampling period, each occurring at slack low tide and into the rising flood. The first event occurs coincidently with the observed temperature rise recorded by the CTD casts and fixed temperature sensors (discussed above; Fig. 7), and is followed by a relatively strong down-welling period. Vertical velocities over the southern pockmark show a more tidally modulated pattern of alternating up- and down-welling periods that extend over much of the water column and into the depths of the pockmark. Upward-directed vertical velocities typically occur during flooding tides, and down-welling currents during the ebb flow.

Figures 9 and 10 show the observed spatial and temporal variation in current magnitude and direction at the rim and center ADCPs of both pockmarks. The variability in vertical

Fig. 7 Time series of sea surface elevation (*top panel*), temperature (*middle panel*), and depth and time averaged vertical velocities below the rim (*bottom panel*). Mean sea surface elevation is from bottom pressure data. The middle panel shows temperature data acquired along the rim (blue) and center (teal) ADCP locations: *solid and dashed lines* RDI Workhorse ADCPs and Aquadopp current meter, respectively. The lower panel shows depth-averaged vertical velocities below the rim averaged over 1 h intervals
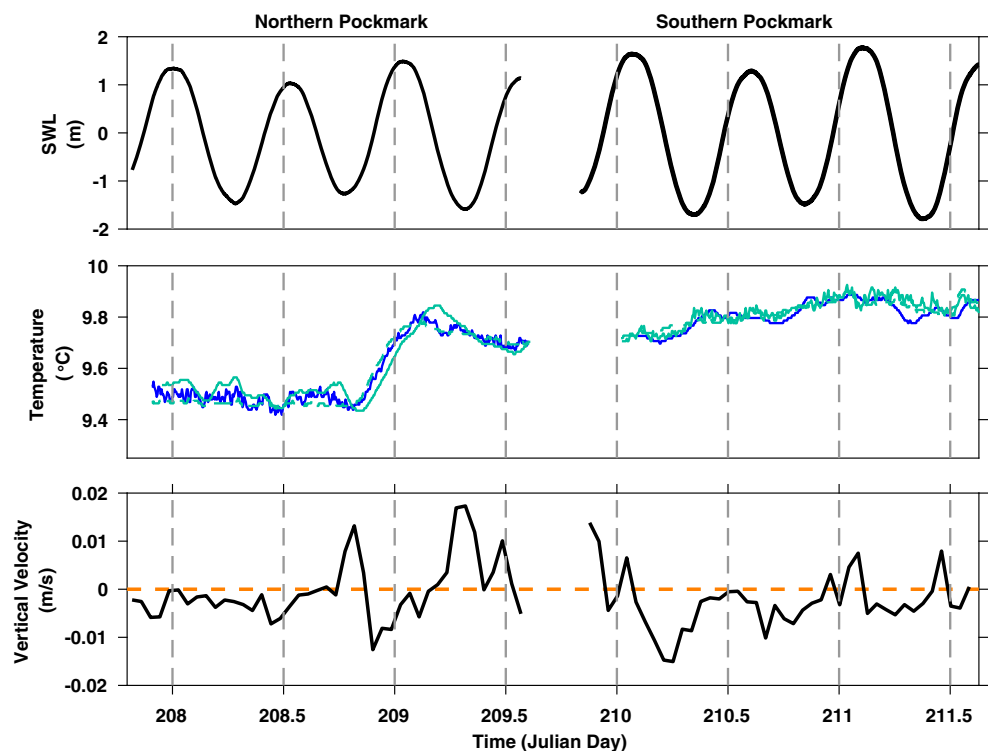
Fig. 8 Hourly averaged vertical velocity data over the northern (*left panel*) and southern pockmark (*right panel*) with the x-axis time in Julian days and the y-axis elevation relative to mean sea level. Vertical velocities range from ±0.02 m/s where positive (negative) values indicate upward (downward) directed flow. *Black lines* Sea surface elevation. *Orange and black dashed lines* Rim and bottom of each pockmark, respectively
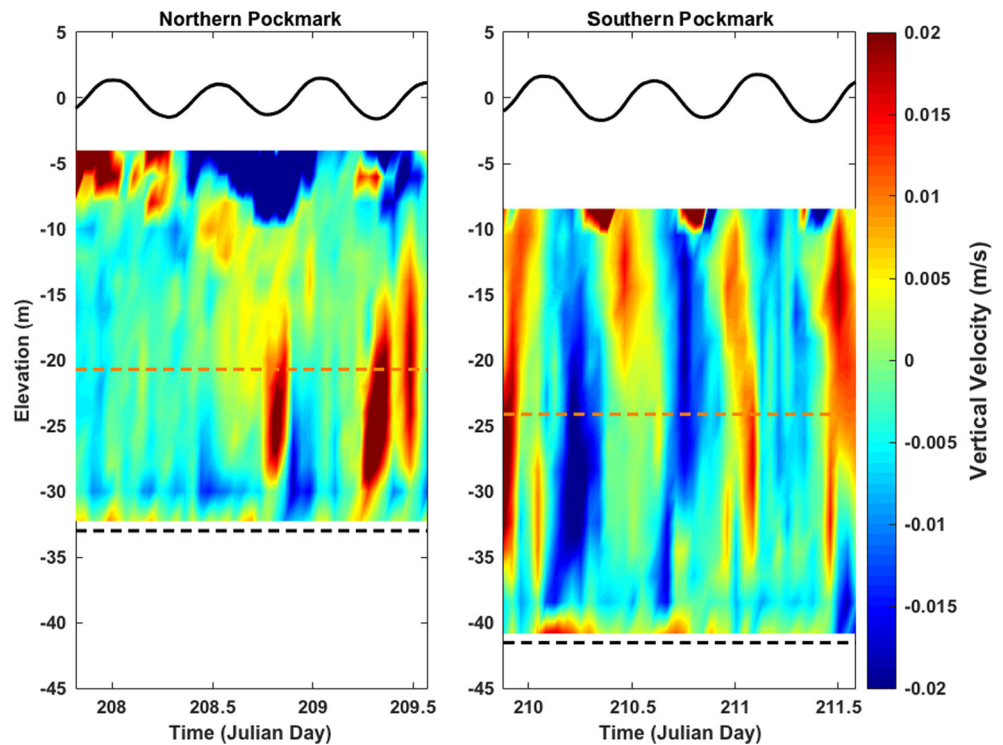

Fig. 9 Hourly averaged current magnitude (*top panels*) and direction (*bottom panels*) data acquired over the northern pockmark at the rim (*left panels*) and center (*right panels*) current meter mounts. The x axis denotes time (Julian day) and the y axis shows elevation relative to mean sea level. Current direction measured in degrees true north. *Orange and black dashed lines* Rim and bottom depths, respectively
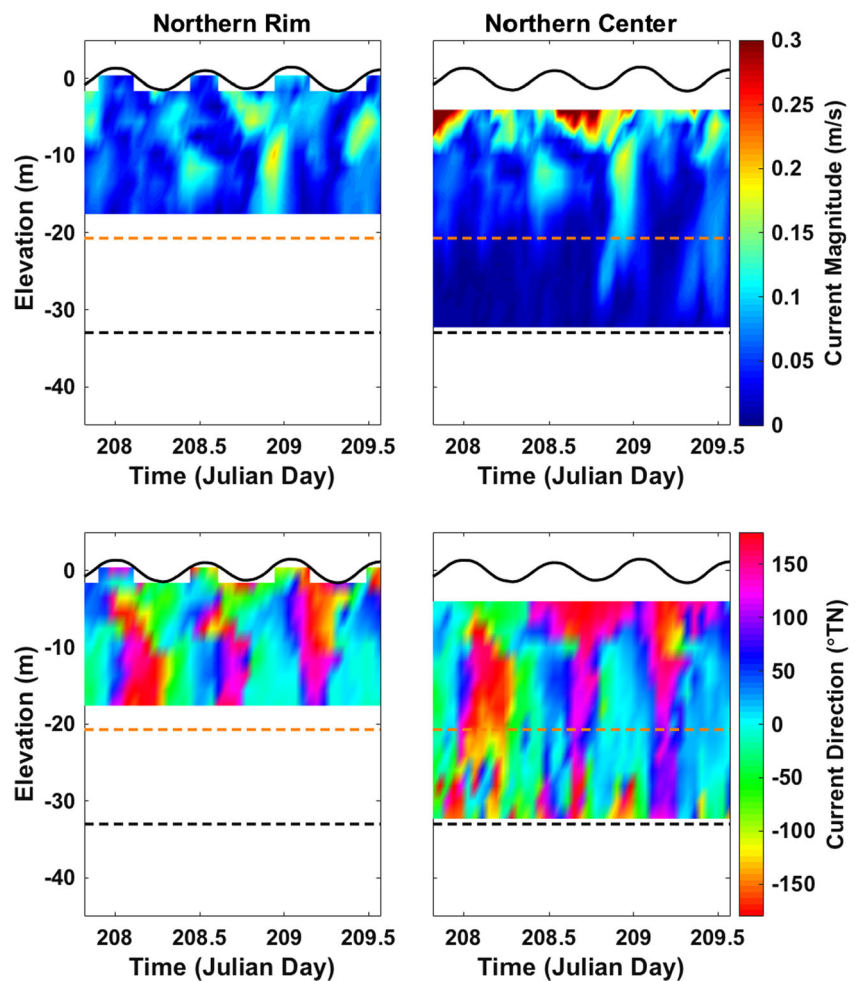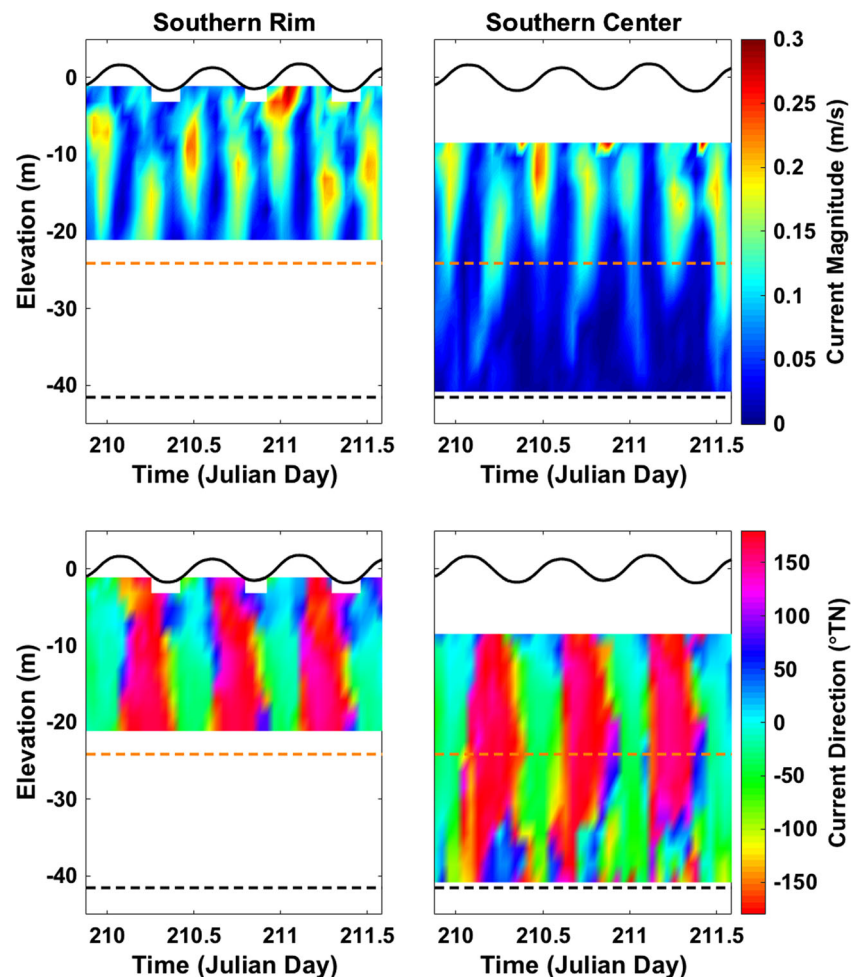
Fig. 10 Hourly averaged current magnitude (*top panels*) and direction (*bottom panels*) data acquired over the southern pockmark at the rim (*left panels*) and center (*right panels*) current meter mounts with the same layout as Fig. 9

structure was greater over the northern pockmark, perhaps due to the winds (Fig. 4), shallower depths (Fig. 2), and convergence of currents around Islesboro Island. In general, current velocities decrease in magnitude with depth, and show increased complexity in rotational (directional) structure below the rim. Surface currents are strongly influenced by transient changes in wind stress and show substantial variability in direction. Upper-water column flow often rotates nearly 180° clockwise (or counterclockwise) from the rim to the center, showing a complex horizontal rotational structure across the pockmark. High-velocity mid-water column currents are tidally modulated with distinct sub-surface maxima over both pockmarks. Moreover, the depth of the sub-surface maximum oscillates with the tidal phase and with pockmark location, occurring at deeper (15 m) depths on rising tides in the north (Fig. 9) and falling tides in the south (Fig. 10), and shallower (5 m) depths on falling tides in the north (Fig. 9) and rising tides in the south (Fig. 10). Mid-depth currents often protrude below the rim and extend downward close to the bottom of the pockmarks.

Lower velocity flows below the rim do not exceed 0.10 m/s, and have significant spatial and temporal variability in

rotational structure. Current direction below the rim rotates both clockwise and counterclockwise with depth, and often exceeds 90° of rotation from the rim to the bottom of the pockmark. A counterclockwise directional pattern is consistently observed over the southern pockmark, whereas the directional structure over the northern pockmark is more variable.

Discussion

Mixing

Temperature, salinity, and density profiles reveal a homogeneous water mass below about 15 m, indicative of a well-mixed lower water column (Figs. 5 and 6). The absence of vertical density gradients below this depth allows small mixing events to strongly affect the temperature profile well into the pockmark. A near-simultaneous 0.3 °C rise in temperature was recorded by temperature sensors along the rim and center ADCPs of the northern pockmark (Fig. 7), an event that occurred coincidently with strong up-welling followed by

down-welling below the rim (Fig. 8). This mixing event is similar in character to observations reported by Manley et al. (2004) of overturning within a freshwater pockmark in Burlington Bay, Lake Champlain, Vermont. They observed increased wind stress at the surface that resulted in rapid cooling of the entire water column due to the replacement of warm, surface water by cold, deep water. This decrease in temperature was associated with strong negative vertical velocities that circulated water throughout the pockmark to create a homogeneous profile. Observations that temperature changes above and below the rim occurred concurrently with strong vertical velocity events indicate that active mixing and overturning may be common under ordinary conditions within Belfast Bay pockmarks.

Further evidence for mixing within pockmarks is provided by observations of strong up- and down-welling events that extended from above the rim down into the pockmark (Fig. 8). Highest magnitude vertical velocities (order 0.015 m/s) typically occur slightly below the rim of the pockmark, presumably due to inner-pockmark circulation patterns. These vertical velocities are similar to numerically modeled results of flow over a pockmark obtained by Hammer et al. (2009). They observed highest vertical velocities within the modeled pockmark that decreased in magnitude toward the surface and were induced by the geometry of the depression. Stronger vertical velocities observed within the Belfast pockmarks are consistent with internal mixing enhanced by pockmark geometry. As well, upwelling currents were observed by Pau et al. (2014) with laboratory experiments using towed physical models of pockmarks (with geometry similar to that of the present study).

Mean current structure

Current structure is subdivided into three distinct layers including a wind-driven surface flow, a tidally modulated midwater flow, and a highly variable deep flow. Flooding tidal conditions typically show a near-northerly flowing surface current that rotates 50–90° with depth, whereas ebbing tidal conditions often show greater directional changes with depth that occur more abruptly, typically reaching 180° about 5–10 m above the seafloor. Comparatively, the current structure over the northern pockmark exhibits greater vertical and temporal variability than over the southern pockmark, which may be related to the geometry of Belfast Bay. Observations of a more complex rotational structure in the northern region of Belfast Bay are consistent with the three-dimensional circulation model of Penobscot Bay developed by Xue et al. (2000). The modeled trajectories of particles released south of Deer Island show both clockwise and counterclockwise circulation around Islesboro Island during summer 1998 conditions at surface (6–10 m) and mid-water (30–40 m) depths (Xue and Brooks 2000). These observations suggest converging tidal

currents around Islesboro Island may describe the circulation pattern within Belfast Bay as well as explain the more complex vertical structure observed over the northern pockmark. Conversely, the proximity of the southern pockmark to the narrow channel to the west of Islesboro Island results in tidally driven currents that align with the channel.

Form drag

The influence of pockmark geometry on the local flow structure was further investigated by examining individual horizontal velocity profiles over each pockmark. Currents over large roughness elements are retarded by contributions from skin friction and form drag. Skin friction refers to the tangential stress at the boundary, whereas form drag results from pressure differences across the object and is produced by flow separation and internal wave generation (McCabe et al. 2006). Chriss and Caldwell (1982) were among the first to describe observations of form drag within subaqueous horizontal velocity profiles. Their observations of multiple logarithmic regions within the velocity profile with slopes that increased with distance from the bed suggest that turbulent stress farther from the bed was greater than it was closer to the seafloor, and that boundary layer flow was significantly influenced by form drag.

Evidence for the influence of form drag on the local flow was investigated by examining the hourly averaged horizontal velocity profiles obtained from the ADCPs at the center of each pockmark (Fig. 11). The nature of the vertical structure in horizontal flow can be examined by identifying periods of logarithmic current structure near the seabed. A fully turbulent boundary layer forms due to the development of turbulent eddies close to the seafloor, a result of the overriding flow experiencing friction with the bed. A turbulent boundary layer flow can be characterized by a logarithmic velocity profile emanating from the seafloor, assuming a no slip condition at the bed (Tennekes and Lumley 1972). This logarithmic velocity profile is modeled as a function of friction velocity (u_*) and height (z) above the bottom, with

$$U(z) = \frac{u_*}{k}\ln\left(\frac{z}{z_o}\right) \qquad (1)$$

where $U(z)$ is the velocity at height z above the bottom, $k=0.41$ is the von Karman coefficient, and z_o is the roughness length scale that varies with grain size and bedform characteristics. Logarithmic regions were identified in this study using a simple, semi-automated algorithm that compared the observed velocity profile to a linear modeled profile in logarithmic space. Following Chelton (1983), the skill, S, used to assess the agreement between the model and observations was determined by the fraction of

Fig. 11 Example hourly averaged horizontal velocity profiles obtained over the southern pockmark and plotted against the log of the vertical distance above the bottom. The y axis is elevation (in m) above the bottom and the x axis is current magnitude (in m/s). Profiles show observations of no logarithmic region (*left panel*), a single logarithmic region (*middle panel*), and a dual logarithmic region (*right panel*). *Horizontal orange dashed line* Rim location
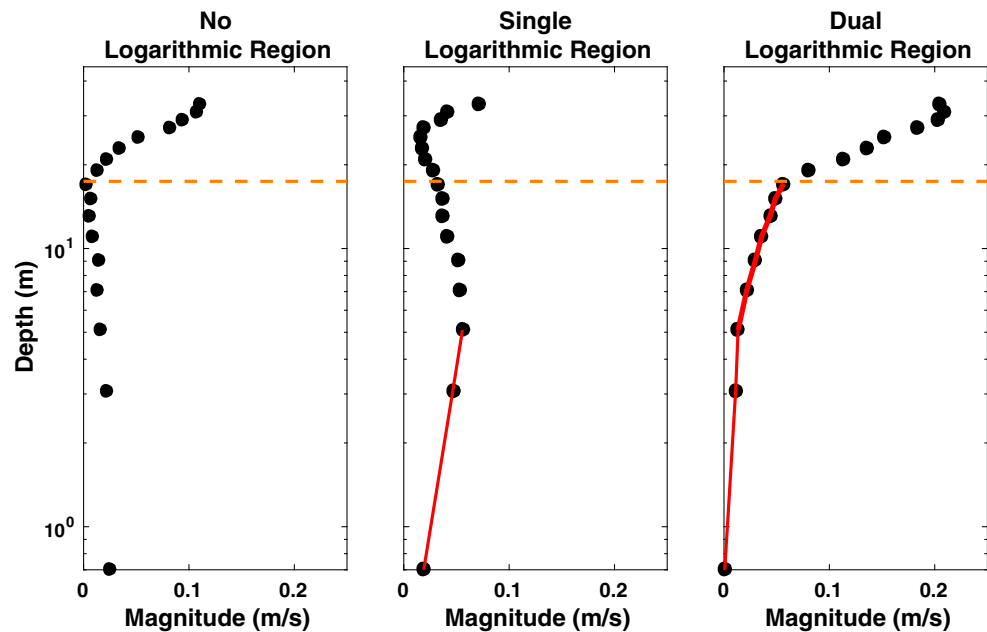
variance explained by the model (equivalent to the correlation squared of an unbiased regression) computed as

$$S = \left(\frac{\sum \left(U(z)_{\text{model}} - \overline{U(z)_{\text{model}}} \right)^2 / N}{\sum \left(U(z) - \overline{U(z)} \right)^2 / N} \right) \qquad (2)$$

where $U(z)$ and $U(z)_{\text{model}}$ are the horizontal velocity profiles of the observed and modeled data, respectively, and N is the number of measurements within the profile. Modeled profiles comprised of three or more data points, with a positive slope, and with skill less than two standard deviations from the skill mean were defined as having a logarithmic region near the bed; all other profiles were characterized as non-logarithmic. For profiles with a logarithmic profile, a second model was applied to data further up in the water column beginning at the highest velocity observation of the first logarithmic layer. In this manner, if present, a second log layer could be identified. The presence of a second logarithmic layer is indicative of form drag resulting from turbulent processes generated by roughness elements of some kind (perhaps other pockmarks) located upstream of the velocity measurements (Arya 1975).

The boundary layer assessment is based on relatively few data points, and thus has relatively large uncertainty in adequately distinguishing logarithmic profiles from linear (or other) profiles. Tests were conducted in an attempt to quantify the fit to the data and led to the semi-automated assessment based on two standard deviations from the skill mean. The presence of what appear to be profiles not inconsistent with single and dual log layers was qualitatively discriminated with the methods. With qualification that there is some uncertainty in the assessment of the current profiles, form drag was observed in the vicinity of the sampled pockmarks consistent with observations of dual logarithmic layers occurring within individual horizontal velocity profiles. The presence of evidence consistent with form drag in this region of Belfast Bay would most likely originate from turbulent processes occurring over nearby, upstream pockmarks. The absence of additional current observations up- and downstream of the pockmarks limits further assessment of the influence by distant features.

Horizontal velocity profiles over the northern and southern pockmarks indicate periods where observations

Fig. 12 Occurrences of observed single and dual logarithmic regions over the center of the northern and southern pockmark. Profiles observed to have a single (dual) logarithmic region are denoted by a *gray* (*black*) square
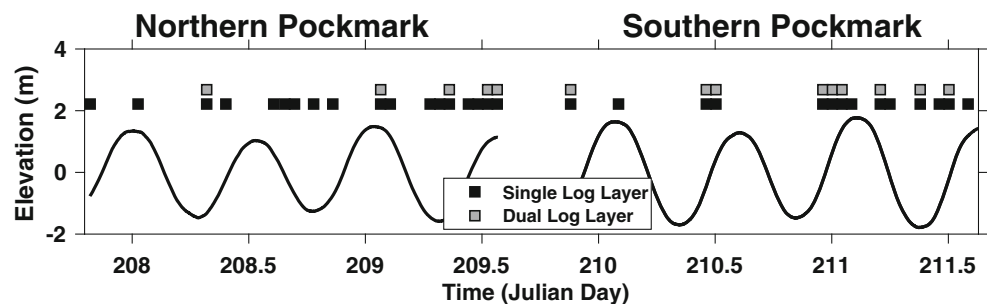
are consistent with no logarithmic region, a single logarithmic region, and a dual logarithmic region (Fig. 12). A greater frequency of single logarithmic regions are observed within the hourly averaged horizontal velocity profiles over the northern pockmark, yet a second logarithmic region is more regularly observed over the southern pockmark (Fig. 12). The second logarithmic region consistently occurs during flood tides over both pockmarks, and may be related to the higher magnitude tidal flows during this time.

Similar to observations obtained by Chriss and Caldwell (1982), the vertical gradient of the upper logarithmic region over the sampled pockmarks is always greater than the lower logarithmic region and suggests that, in the presence of nearly uniform density structure, roughness-induced form drag could be contributing to the total boundary stress over the sampled pockmarks. Extending over a large portion of the water column, these logarithmic regions are consistent with active mixing in the vicinity of pockmarks. Additional current observations at control sites (not acquired) located at increasing distances from the pockmark field would be useful to further examine the spatially varying influence of form drag over the field of Belfast pockmarks.

Conclusions

Temperature, salinity and current observations acquired over two pockmarks in Belfast Bay, Maine indicate active mixing and overturning within the depressions and are consistent with enhanced turbulence due to roughness-induced form drag. Evidence of active overturning within the sampled pockmarks was observed from uniform temperature and density profiles within the pockmarks, and a nearly simultaneous rise in temperature at the rim and center of the northern pockmark that occurred coincidentally with strong vertical velocities extending from the rim down into the pockmark. This observed overturning event has implications for nutrient distribution within pockmarks whereby nutrient-rich surface waters may be transferred to depth to support benthic communities. Enhanced turbulence observed in the sampled pockmarks, in conjunction with the higher velocity flows and elongated geometry of the southern pockmark, suggest near-bed flow may be acting to modify pockmark geometry over time.

The incorporation of a control site uninfluenced by pockmark geometry would better evaluate the results of this study and provide a comparative data set to the pockmark observations obtained herein. Future studies should include long-term monitoring of the temperature and current patterns over multiple pockmarks and separate control sites to assess the influence of storm events on the vertical structure above pockmarks and better constrain nutrient, circulation, and sediment transport patterns within these depressions.

Compliance with ethical standards

Conflict of interest The authors declare that there is no conflict of interest with third parties.

References

Andrews BD, Brothers LL, Barnhardt WA (2010) Automated feature extraction and spatial organization of seafloor pockmarks, Belfast Bay, Maine, USA. Geomorphology 124:55–64

Arya SPS (1975) A drag partition theory for determining the large-scale roughness parameter and wind stress on the arctic pack ice. J Geophys Res 80:3447–3454

Brothers LL, Kelley JT, Belknap DF, Barnhardt WA, Andrews BD, Maynard ML (2011a) More than a century of bathymetric observations and present-day shallow sediment characterization in Belfast Bay, Maine, USA: implications for pockmark field longevity. Geo-Mar Lett 31:237–248

Brothers LL, Kelley JT, Belknap DF, Barnhardt WA, Koons PO (2011b) Pockmarks: self-scouring seep features? In: Proc 7th Int Conf Gas Hydrates, 17–21 July, Edinburgh, UK

Brothers LL, Kelley JT, Belknap DF, Barnhardt WA, Andrews BD, Legere C, Hughes Clarke JE (2012) Shallow stratigraphic control on pockmark distribution in north temperate estuaries. Mar Geol 329–331:34–45

Chelton DB (1983) Effects of sampling errors in statistical estimation. Deep Sea Res 30:1083–1103

Chriss TM, Caldwell DR (1982) Evidence for the influence of form drag on bottom boundary layer flow. J Geophys Res 87:4148–4154

Christodoulou D, Papatheodorou G, Ferentinos G, Masson M (2003) Active seepage in two contrasting pockmark fields in the Patras and Corinth Gulfs, Greece. Geo-Mar Lett 23:194–199

Fandel CL, Lippmann TC, Foster DL, Brothers LL (2016a) Observations of pockmark flow structure in Belfast Bay, Maine, Part 2: evidence for cavity flow. Geo-Mar Lett, this volume. doi:10.1007/s00367-016-0473-3

Fandel CL, Lippmann TC, Foster DL, Brothers LL (2016b) Observations of pockmark flow structure in Belfast Bay, Maine, Part 3: implications for sediment transport. Geo-Mar Lett, this volume. doi:10.1007/s00367-016-0474-2

Gay A, Lopez M, Ondreas H, Charlou JL, Sermondadaz G, Cochonat P (2005) Seafloor facies related to upward methane flux within a giant pockmark of the lower Congo Basin. Mar Geol 226:81–95

Hammer Ø, Webb KE, Depreiter D (2009) Numerical simulation of upwelling currents in pockmarks, and data from the Inner Oslofjord, Norway. Geo-Mar Lett 29:269–275

Hovland M, Judd A (1988) Seabed pockmarks and seepages: impact on geology, biology, and the marine environment. Graham and Trotman, London

Hovland M, Svensen H (2006) Submarine pingoes: indicators of shallow gas hydrates in a pockmark at Nyegga, Norwegian Sea. Mar Geol 228:15–23

Hovland M, Svensen H, Forsberg CF, Johansen H, Fichler C, Fosså JH, Jonsson R, Rueslåtten H (2005) Complex pockmarks with carbonate-ridges off mid-Norway: products of sediment degassing. Mar Geol 218:191–206

Kelley JT, Dickson SM, Belknap DF, Barnhardt WA, Henderson M (1994) Giant sea-bed pockmarks: evidence for gas escape from Belfast Bay. Geology 22:59–62

Kilhams B, McArthur A, Huuse B, Ita E, Hartley A (2011) Enigmatic large-scale furrows of Miocene to Pliocene age from the central North Sea: current-scoured pockmarks? Geo-Mar Lett 31:437–449

Manley PL, Manley TO, Watzin MC, Gutierrez J (2004) Lakebed pockmarks in Burlington Bay, Lake Champlain: I. Hydrodynamics and implications of origin. In: Manley TO, Manley PL, Mihuc TB (eds) Lake Champlain: partnerships and research in the new millennium. Springer, Berlin, pp 299–330

McCabe RM, MacCready P, Pawlak G (2006) Form drag due to flow separation at a headland. J Phys Oceanogr 36:2136–2152

Pau M, Hammer O (2013) Sediment mapping and long-term monitoring of currents and sediment fluxes in pockmarks in the Oslofjord, Norway. Mar Geol 346:262–273

Pau M, Gisler G, Hammer Ø (2014) Experimental investigation of the hydrodynamics in pockmarks using particle tracking velocimetry. Geo-Mar Lett 34:11–19

RD Instruments (2005) Workhorse acoustic Doppler current profiler technical manual. RD Instruments P/N957-6150-00, pp 196

Ritt B, Pierre C, Gauthier O, Wenzhöfer F, Boetius A, Sarrazin J (2011) Diversity and distribution of cold-seep fauna associated with different geological and environmental settings at mud volcanoes and pockmarks of the Nile Deep-Sea Fan. Mar Biol 158:1187–1210

Rogers JN, Kelley JT, Belknap DF, Gontz A, Barnhardt WA (2006) Shallow-water pockmark formation in temperate estuaries: a consideration of origins in the western gulf of Maine with special focus on Belfast Bay. Mar Geol 225:45–62

Scanlon KM, Knebel HJ (1989) Pockmarks in the floor of Penobscot Bay, Maine. Geo-Mar Lett 9:53–58

Tennekes H, Lumley JL (1972) A first course in turbulence. IBM Univ Medium, USA

US Geological Survey (2010) Stream gauge data. http://waterdata.usgs.gov/me/nwis

Weather Underground, Inc. (2011) http://www.wunderground.com

Wildish DJ, Akagi HM, McKeown DL, Pohle GW (2008) Pockmarks influence benthic communities in Passamaquoddy Bay, Bay of Fundy, Canada. Mar Ecol Prog Series 357:51–66

Xue H, Brooks D (2000) Characterization of fronts and eddies in Penobscot Bay using a three-dimensional ocean circulation model. Final Report presented to Island Institute, Rockland, ME

Xue H, Xu Y, Brooks H, Pettigrew N, Wallinga J (2000) Modeling the circulation in Penobscot Bay, Maine. Estuarine and Coastal Modeling. In: Proc 6th Int Conf, American Society of Engineers, New Orleans, LA